Construction and Building Materials 274 (2021) 121837

Contents lists available at ScienceDirect

Construction and Building Materials

journal homepage: www.elsevier.com/locate/conbuildmat

Factors affecting the detectability of concrete delamination in GPR images

Kien Dinh [a,*], Nenad Gucunski [b]

[a] NDT Concrete LLC, FL, USA
[b] Department of Civil & Environmental Engineering, Rutgers University, NJ, USA

HIGHLIGHTS

- The study aimed to understand the potential of GPR in detecting concrete delamination.
- It explored various factors that might affect the detectability of concrete delamination.
- The study was conducted using both synthetic and real GPR data from concrete slab.
- It was found that GPR has a great potential to be used as a delamination detection tool.
- The detectability of a delamination is affected by some factors described in the paper.

ARTICLE INFO

Article history:
Received 9 August 2020
Received in revised form 12 November 2020
Accepted 21 November 2020
Available online 4 December 2020

Keywords:
GPR
Concrete
Delamination
Inspection
Condition assessment

ABSTRACT

Concrete delamination is a common type of defects in concrete bridge decks and rigid pavements. While it was reported that ground-penetrating radar (GPR) was able to visualize such types of defects in many instances, it is still unclear about the conditions of success for that application. In such a context, this study aimed to explore various factors that might affect the detectability of concrete delamination in GPR images/signals. In terms of methodology, the study was conducted using both synthetic data generated from a GPR simulation program, and real data collected on a concrete slab specimen. The analysis of such image data revealed the following. First, there is always a waveform reflected from concrete delamination. However, its strength is affected mainly by the thickness of the delamination, the material (air or water) within it, and the peak (most energetic) frequency of the emitted signal. Second, the depth of delamination and its location relative to neighboring steel bars might impact its detectability in GPR images.

1. Introduction

Concrete delamination is a common type of distress in concrete bridge decks and rigid pavements. Concerning the mechanisms, while delamination in bridge decks is usually a result of corrosion of reinforcing steel [1–2], the same in rigid pavements often occurs as a result of differential shrinkage stresses in concrete [3]. Regardless of the mechanism, if repairs are not made in a timely manner, delamination will finally develop into open spalls that reduce the ride quality and the integrity of the structure [1–3]. Due to that reason, it is necessary to have effective methods for the detection and monitoring of the progression of existing delaminations.

Ground-penetrating radar (GPR) has long been identified as a potential nondestructive evaluation (NDE) technology that might help solve the above problem. For instance, the earliest study in the United States that targeted using GPR to image concrete delamination in bridge decks dates back to the year 2001 [4]. Continuing efforts have been made for both bridge decks [5–6] as well as for rigid pavement [7]. Unfortunately, the mixed results reported in those studies have led to the impression that GPR is unable to directly image the presence of delamination [1]. Motivated by both past reported successes and failures, this study aimed at understanding the factors that may influence the effectiveness of GPR for detecting concrete delamination.

It was determined from the start that numerical simulation would be used in the first step to investigate the problem. Once the promising indicators of delamination detection have been identified from the numerical studies, real data will be collected to verify them. As one can realize, numerical simulations offer

* Corresponding author.
E-mail addresses: kien@ndt-concrete.com (K. Dinh), gucunski@soe.rutgers.edu (N. Gucunski).

https://doi.org/10.1016/j.conbuildmat.2020.121837
0950-0618/

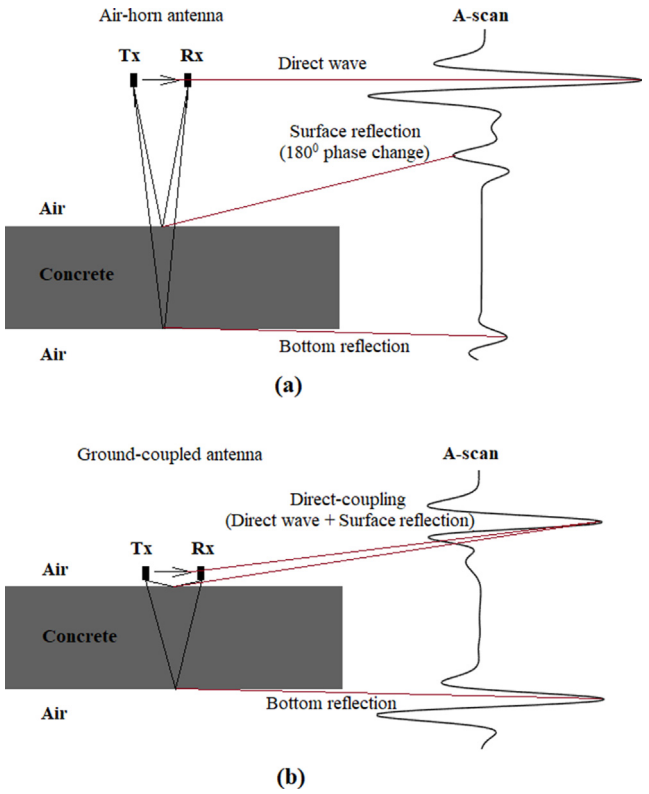

Fig. 1. A-scan of a signal received by (a) an air-coupled and (b) a ground-coupled antenna.

two significant benefits. First, they allow us to understand the behavior of the physical world without the need to build real objects or buy equipment. Second, they help us to see whether it is worth conducting a physical experiment or to come up with the best experiment design. On the other end, a limitation of numerical modeling is that we may not yet fully understand the complexity of an actual element. As a consequence, when building a numerical model, some parameters may have been omitted or simplified.

2. GPR data from concrete structures

Understanding how GPR signals are formed and what are their responses to various scenarios is the most important factor for the success of any GPR application. As such, this section will briefly explain different forms of GPR data display and what parameters may affect their signatures.

2.1. Display of GPR data

To start, an A-scan is the building block of GPR data. It is a waveform collected at a single location. While Fig. 1a depicts an A-scan collected with an air-coupled or horn antenna, Fig. 1b presents the one collected with a ground-coupled GPR antenna. As can be seen, for a horn antenna, there is a certain separation between the direct-wave and surface reflection. On the other hand, for a ground-coupled antenna, those two waveforms are blended to form what is usually called the "direct-coupling" signal. Although this study focused on using a ground-coupled antenna, the operation of the air-coupled antenna is presented in Fig. 1a purposely to explain an important effect, namely "phase reversal." It is a phenomenon observed when an electromagnetic wave is reflected from a medium of higher dielectric constant. In such cases, the wave experiences a phase change of 180^0. Since the dielectric constant of concrete is greater than that of air, the reflection from the concrete surface will change phase 180^0 compared to the transmitted signal.

As can be realized, an A-scan contains mostly one-dimensional information. Therefore, it is only appropriate for displaying GPR data from layered-type structures such as pavements. For concrete with embedded rebars or for other testing scenarios where features are expected to change significantly over the survey line, a B-scan is more frequently used to display the results. It is created by stacking individual A-scans over the length of a survey line. The amplitudes of those A-scans are then converted to pixel intensities to form a two-dimensional image. Fig. 2 presents a typical B-scan for concrete structures obtained with ground-coupled GPR. As can be seen, while its vertical axis indicates the two-way travel time of the signals, its horizontal axis shows the traveling distance of the antenna (the location of each A-scan). Furthermore, it should be noted that the hyperbolic patterns on the B-scan are the signatures of steel reinforcement [8,9].

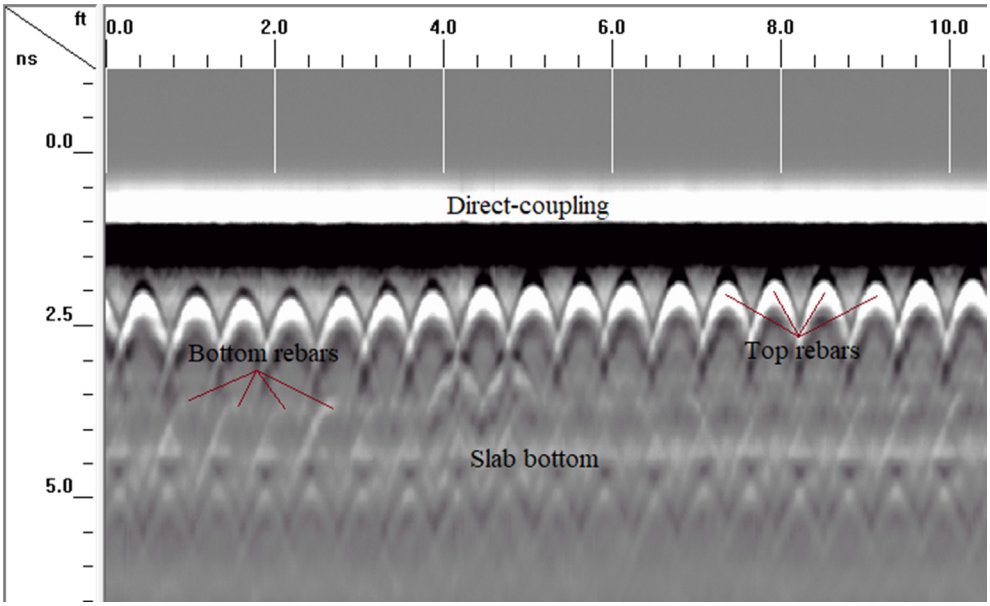

Fig. 2. Typical B-scan from a survey of a concrete slab using a ground-coupled antenna.

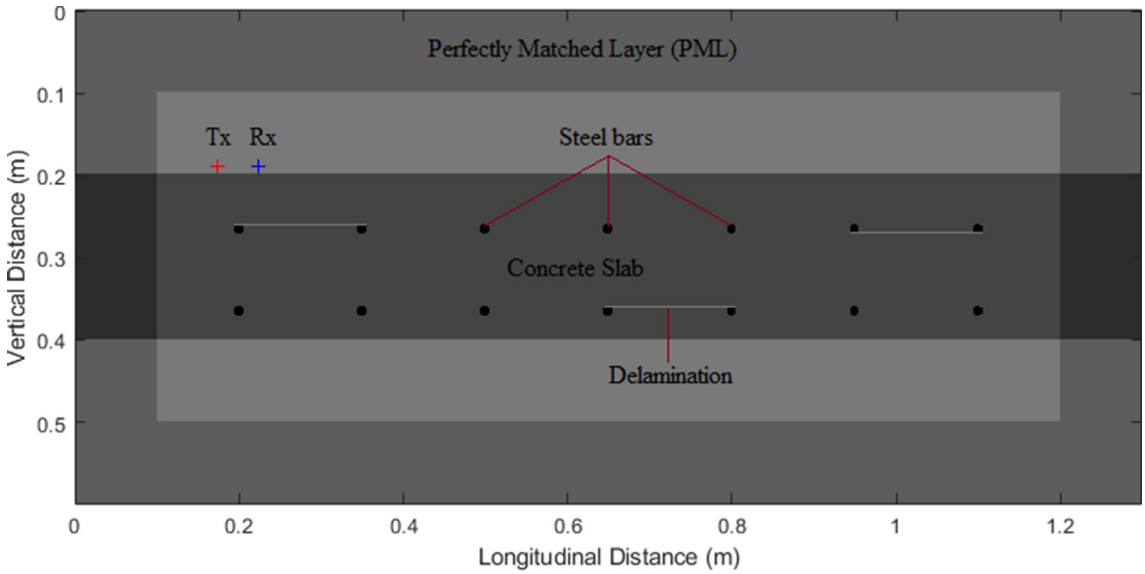

Fig. 3. Example of a simulation experiment with the computational modeling program.

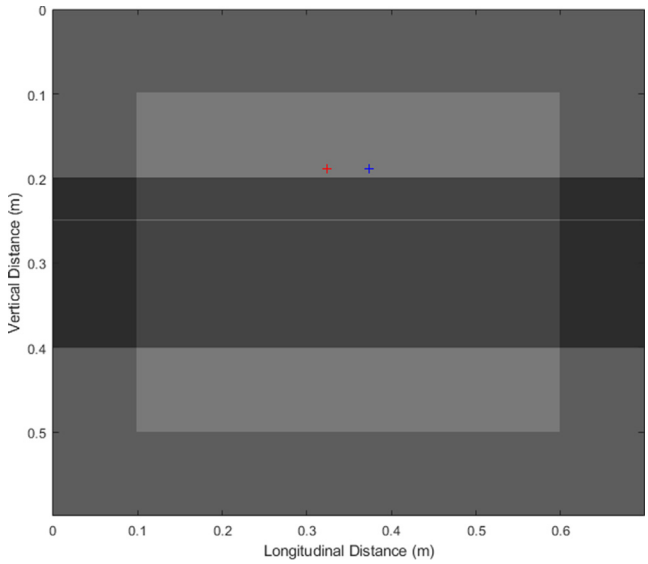

Fig. 4. Simulation setup for studying the effect of delamination thickness.

2.2. Parameters affecting GPR signals

As previously mentioned, the dielectric constant affects the phase of the reflected signal. In addition, it determines the propagation velocity of an electromagnetic wave in a medium. The higher the dielectric constant of a material, the slower GPR signals will travel in that material [10]. This effect can be observed in Fig. 1a when, although the distance from the antenna to the concrete surface is greater than the thickness of the concrete element, the travel time between the top and bottom of the slab is still greater than the one between the antenna and concrete surface. That is because, on average, the dielectric constant of concrete is about nine times greater than that of air or vacuum. Accordingly, GPR signal travels in concrete three times slower than when it travels in the air.

Along with the dielectric constant, electrical conductivity is another important parameter that has a significant effect on GPR signals [10,11]. Specifically, concrete with a higher electrical conductivity will attenuate more electromagnetic energy through inducing eddy currents. According to [11], this attenuation mechanism is called a *conductive loss*. It is different from the *dielectric loss*, which is caused by the damping forces in each atom [11,12]. The effect of the above losses is that they make it more difficult to see reflections from objects in GPR images/signals. Such an effect will increase with the depth of an object.

3. Experiments using numerical simulation

3.1. Description of the simulation program

In this study, a computational modeling program was developed in MATLAB to simulate the use of GPR for concrete inspection. Specifically, the program works by solving Maxwell's curl equations in 2-dimensional (2D) space using the Finite-Difference Time-Domain (FDTD) method. This method was proposed by Yee in 1966 [13], in which he came up with a special design to stagger electric and magnetic vector fields across the computational grid. Such a grid allows Maxwell's curl equations to be solved easily with finite-difference approximation [14,15].

Fig. 3 presents a visualization of the experimental setup in this research using the computational modeling program. As can be seen, in this specific experiment, the concrete slab has a thickness of 20 cm and includes fourteen steel bars. Seven bars are on top, and the other seven are at the bottom. The concrete cover is about 6 cm for the top rebars and 3 cm for the bottom rebars. Three air-filled delaminations of 1 mm thick are embedded in the slab. Tx (red mark) and Rx (blue mark) denote the transmitter and receiver locations, respectively. Furthermore, a Perfectly Matched Layer (PML) is included at the boundary of the computational space to absorb the outgoing waves and prevent them from reflecting toward the receiver location [16]. Finally, although not being indicated in Fig. 3, the Ricker wavelet is used as the transmitted pulse in the program. Since it contains a spectrum [17], the peak (most energetic) frequency is used to define the frequency of an antenna in this research.

3.2. The effect of delamination thickness

It was determined at the beginning of the current research that it would focus firstly on studying the effect of delamination

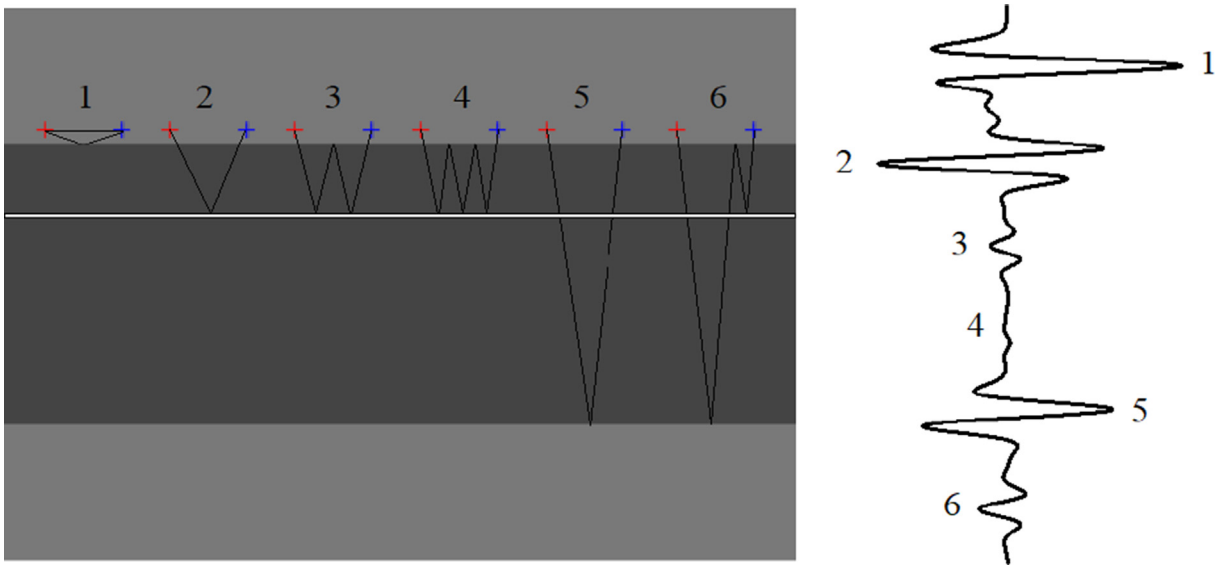

Fig. 5. Schematic explanation of A-scan formation.

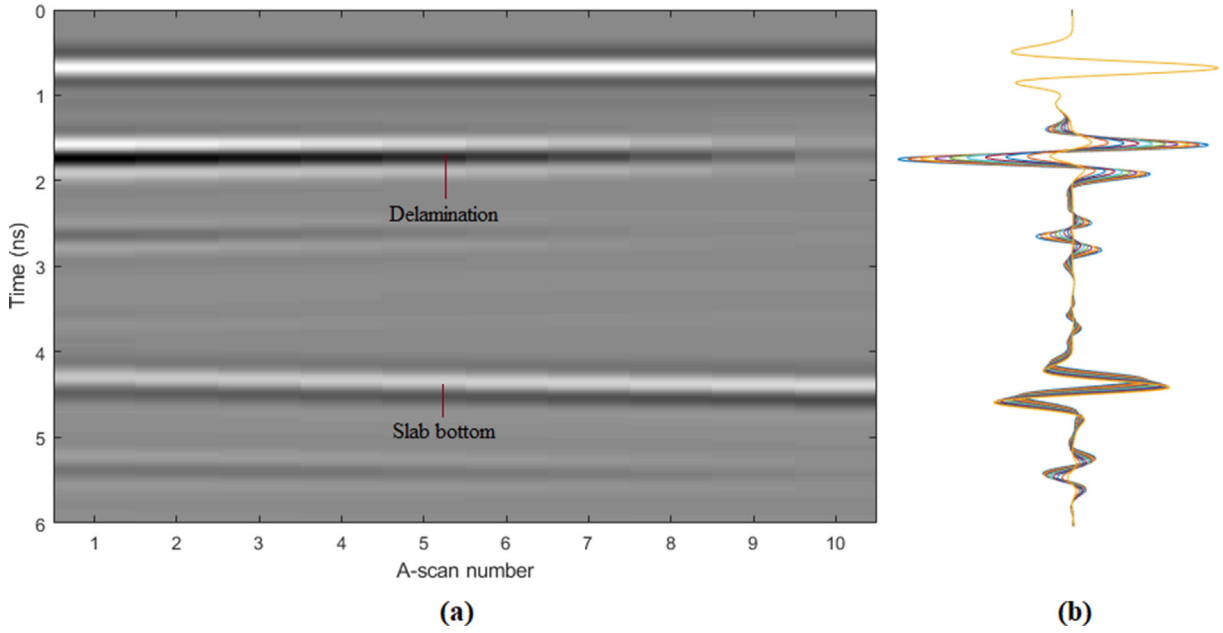

Fig. 6. The effect of delamination thickness observed in (a) B-scan image and (b) A-scans.

thickness on GPR signals. The motivation for it is as follows. First, Scott et al. [4] observed that when the thickness of an air gap between two concrete plates was reduced from 1.3 cm to 1 mm, the response from the air gap in the signal collected by a *prototype* GPR system almost disappeared. Second, Tarussov et al. [10] stated that "only large cracks (2–3 mm or wider) are able to produce reflections or signal attenuation." However, neither one of the studies provided an explanation of why and how the thickness of delamination affects its detectability in GPR images/signals.

To answer the above question, a simulation model was set up, as shown in Fig. 4, using a 2-GHz antenna. The slab in the model is 20 cm thick, and concrete is assigned a typical dielectric constant of 8 and an electrical conductivity being equal to 0.001 S/m. The transmitter and receiver are at 1 cm above the concrete surface. Air-filled delamination is embedded in the slab at a depth of 5 cm. Ten delamination thickness values were used for ten simulation runs. Specifically, 10 mm was used as the starting value, and in each next simulation, the delamination thickness was reduced by 1 mm. Since one A-scan is generated for each simulation, as shown Fig. 5, there is a total of 10 A-scans obtained for this experiment. The scans are stacked together and plotted in the form of both B-scan image and A-scan signals in Fig. 6.

The effect of delamination thickness on GPR images/signals can be clearly observed in Fig. 6. Specifically, the thinner the delamination is, the weaker the signals reflected from it will be. In other words, the thinner delamination is, the more difficult it can be identified in the GPR image. As mentioned earlier, while this phenomenon is known in the literature [4,10], the main interests in this research are (1) to find an explanation for it and (2) to answer whether commonly-used GPR systems can detect delamination of a thickness less than 2 mm. Theoretically, Fig. 6 has positively answered the latter question. Concerning the effect

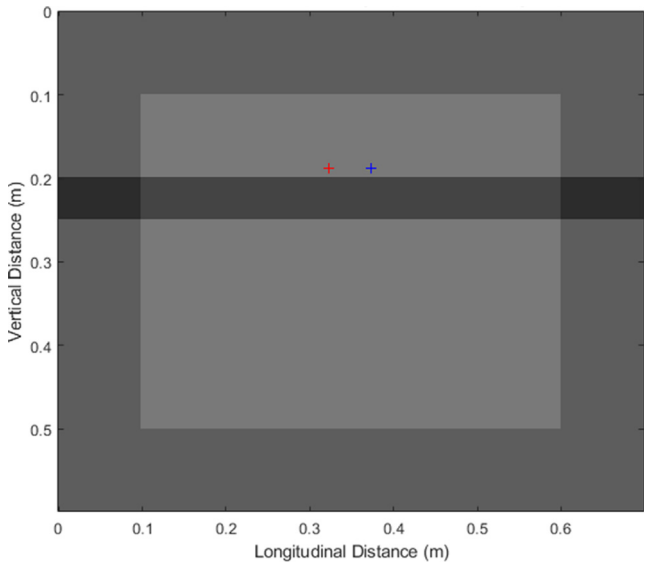

Fig. 7. Simulation setup to obtain the reflection from the concrete/air interface of the delamination.

of delamination thickness, the process to understand and explain it is as follows.

First, when analyzing Fig. 6, one can notice that the shapes of the reflections from the delamination are not similar to the shape of the transmitted waveform (Ricker wavelet), which should resemble the reflections from the slab bottom. This observation has led the authors of this research to a hypothesis that the signal reflected from delamination is a mixture of the following two waveforms. The first waveform is the reflection from the concrete/air interface, and the second waveform is the reflection from the air/concrete interface. As can be realized, the thinner delamination is, the closer the two waveforms will be to each other.

With the above hypothesis, one can explain why the strength of reflection from delamination significantly decreases when reducing its thickness. The reason is the *phase reversal* effect earlier mentioned. It leads to the destructive interference of the two waveforms described above. To be more specific, while the reflection from the concrete/air interface does not change phase 180^0, the one from the air/concrete interface does. The next simulation is presented in support of this explanation. Specifically, Fig. 7 depicts a simulation setup to isolate the reflection from the concrete/air interface of the previous simulation experiment where the thickness of the slab is equal to 5 cm. The A-scan generated in this simulation can then be subtracted from the A-scans in the previous experiment to obtain the waveforms from the air/concrete interface of the delamination. If the above explanation is correct, the following phenomena should be expected.

First, because the dielectric constant of concrete is greater than that of air, the waveforms obtained from such a subtraction should have a phase change of 180^0 at the location of the delamination. Second, since the concrete surface below the air gap (delamination) moves closer to the antenna when the thickness of the delamination is reduced from 10 mm to 1 mm, the strength of the waveforms reflected from it should increase gradually due to

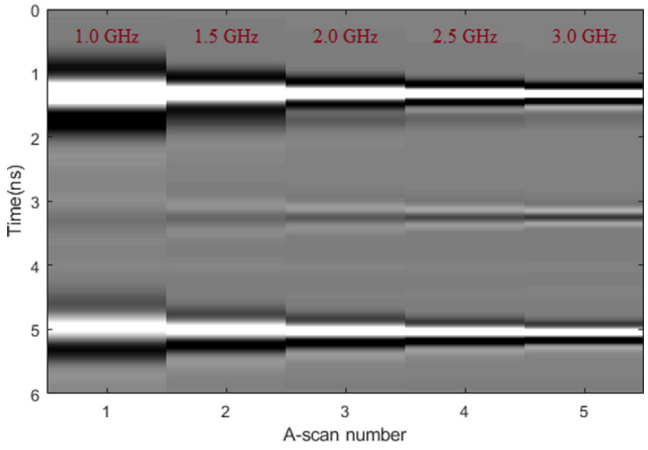

Fig. 9. The effect of GPR frequency on the detectability of 1-mm thick delamination.

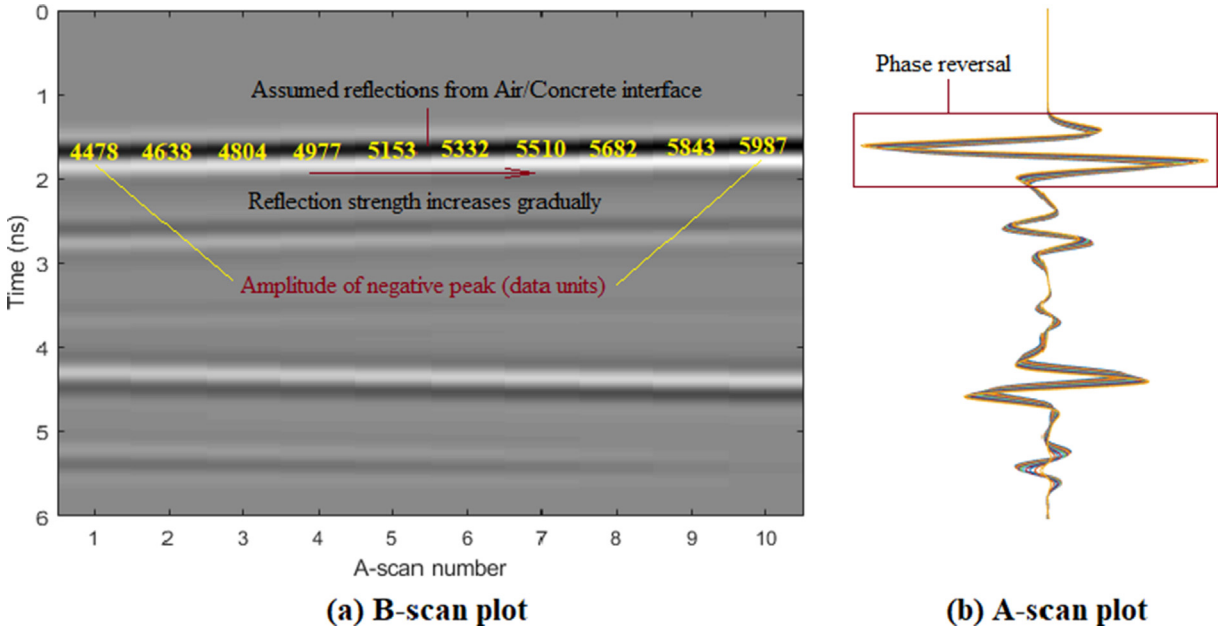

Fig. 8. Assumed reflections from the air/concrete interface of the delamination.

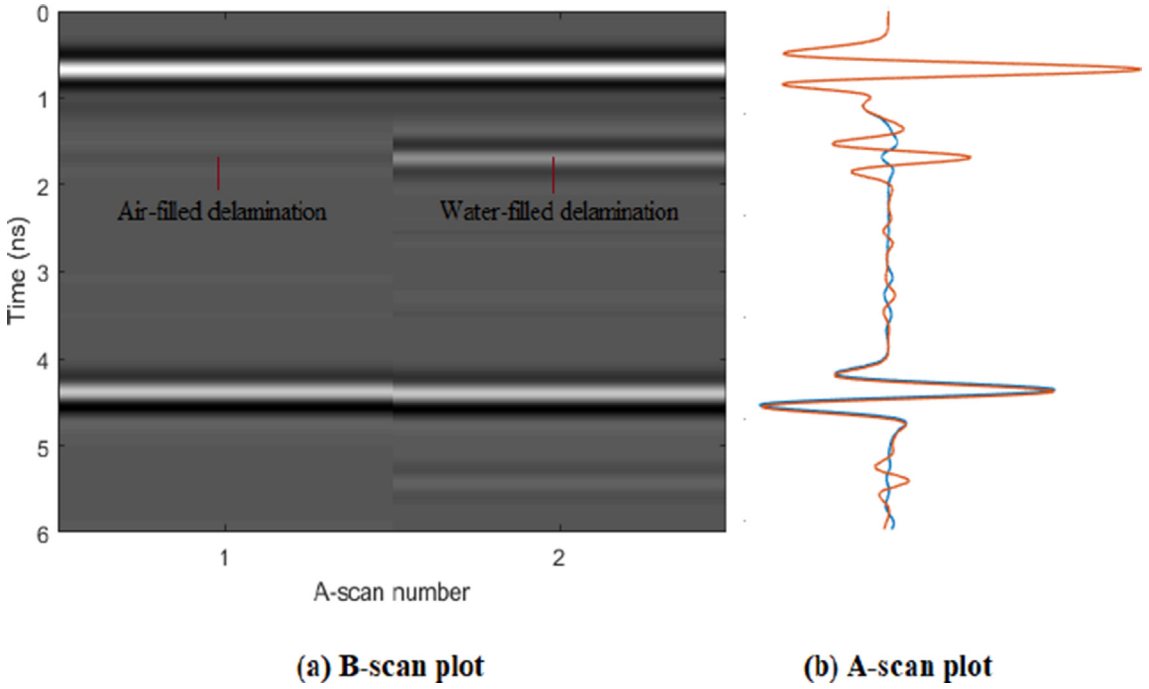

Fig. 10. Simulated GPR images/signals obtained from air-filled and water-filled delamination.

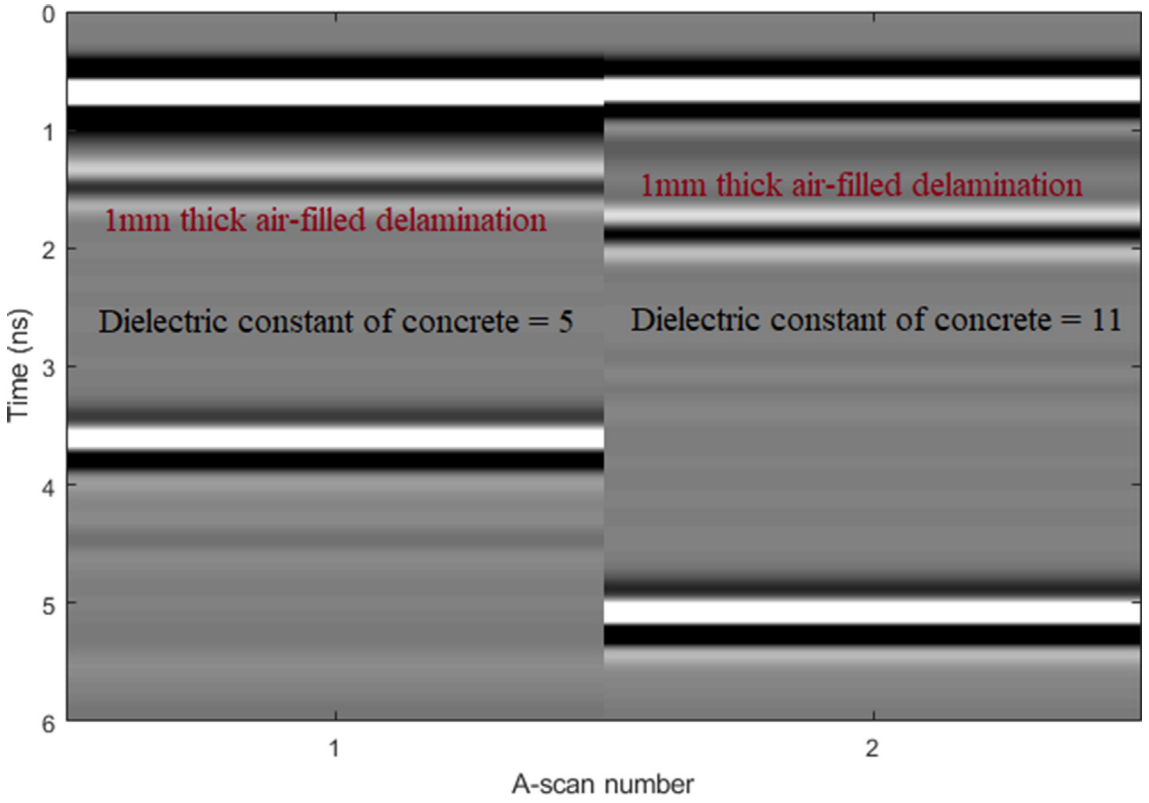

Fig. 11. Effect of dielectric constant of concrete to the detectability of delamination.

geometric loss [11]. As can be seen in Fig. 8, both of these phenomena exist as being expected.

For clarification, first it is noted that the thickness of concrete above the air gap in Fig. 4 is kept constant in the entire experiment, being equal to 5 cm. The thickness of the delamination itself is reduced by raising the concrete surface below the air gap. As such, the thinner the air gap, the closer the concrete surface below it to GPR antennas and accordingly the stronger reflection. Second, the geometric loss mentioned above is the decrease in the strength of electric field due to the inverse-square law. Finally, it is noted that, in this paper, the simulated signals are plotted using raw data without any gain being applied. However, as one may notice, since

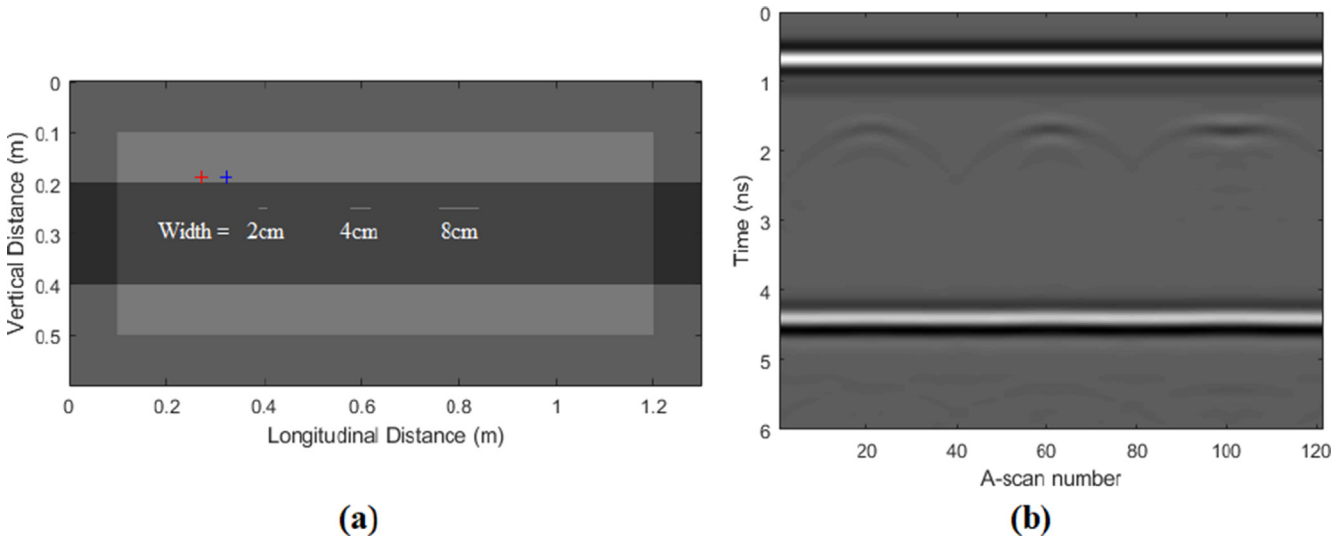

Fig. 12. Effect of delamination width to its detectability.

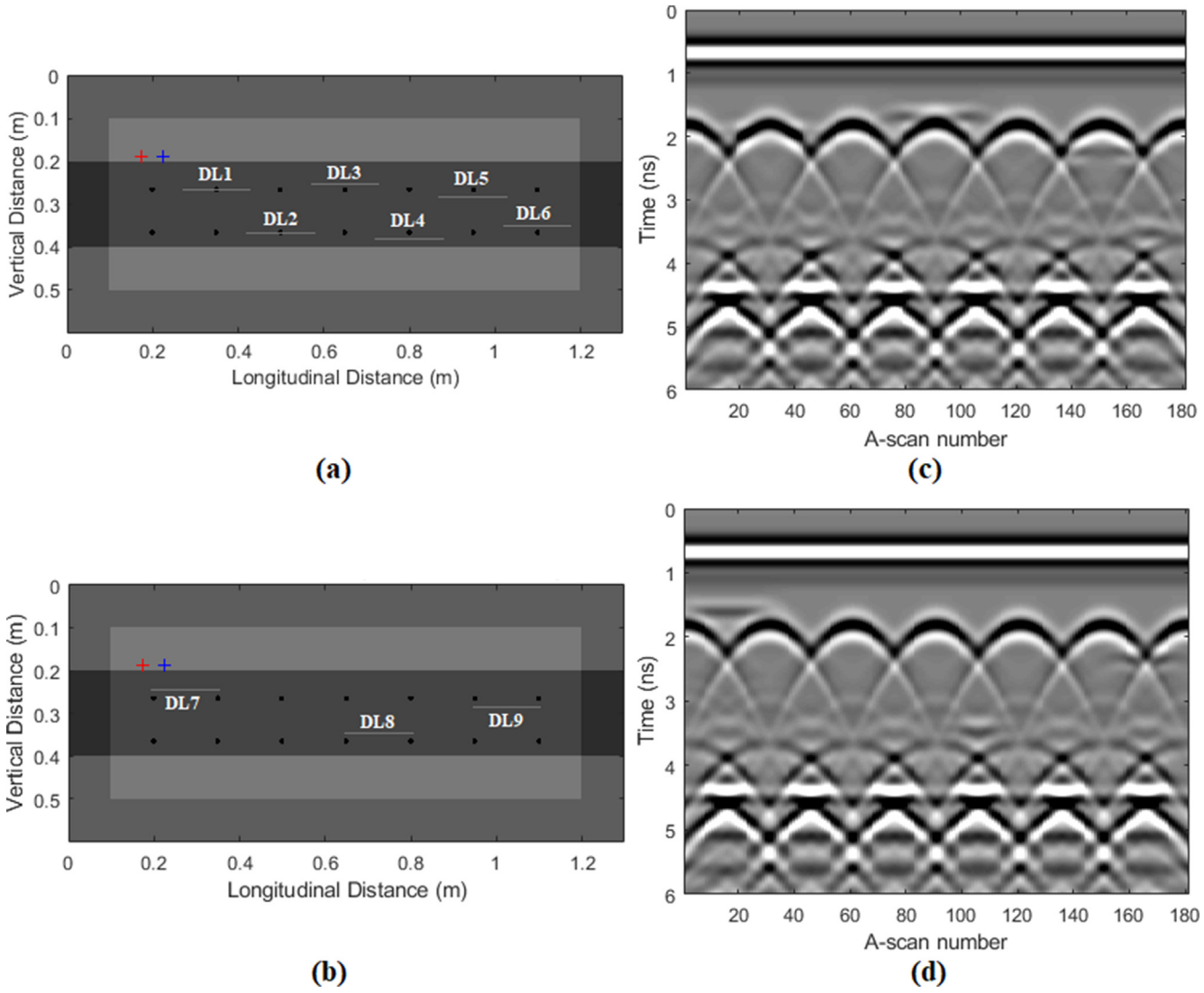

Fig. 13. The effect of steel bars on the detectability of delamination.

Maxwell's curl equations do not take into account frequency-dependent dielectric loss, the signals obtained from the simulations will be attenuated less compared to those collected on real concrete.

3.3. The effect of antenna frequency

Theoretically, it is expected that, for the same delamination, GPR images obtained from a lower frequency antenna will be affected more by the above effect of destructive interference. The reason is a lower frequency pulse will lead to a higher ratio between the wavelength and the thickness of the delamination. Consequently, the reversal of the waveform reflected from the air/-concrete interface will become closer in phase with the waveform from the concrete/air boundary's reflection. Results in Fig. 9 confirm such a theory when five different frequencies (1.0–3.0 GHz) were used in turn for a simulation. In the simulation, 1 mm thick delamination was embedded right at the middle height of a 20 cm thick concrete slab. In combination with the results in Fig. 6, those in Fig. 9 lead us to the following definition of a dimensionless factor to define the detectability of delamination. Specifically, if the ratio between the wavelength of the GPR signal (when traveling in concrete) and delamination thickness is less than 50, it is likely that the delamination will appear clearly in the B-scan image. In other words, one can say that a 2 GHz antenna will provide equally good detection of a 1 mm delamination, as a 1 GHz antenna will do for a 2 mm thick delamination. However, it should be noted that, if a delamination is close to concrete surface and the frequency of transmitted signals is small enough, there may be a resolution problem that will affect the detectability of delamination. Specifically, in such cases, there will be a mixture between two wavelets, i.e., one from the concrete surface and the other from the delamination.

3.4. Water-filled versus air-filled delamination

It has been reported in the literature that water-filled delamination may produce a stronger reflection than the one filled with air [18]. To verify that assumption, the simulation setup, as the one shown in Fig. 4, is used again with two modifications. First, the thickness of the delamination is reduced further to 0.2 mm. Second, two values are employed in turn for its dielectric constant. The value of 1 is used to simulate air-filled delamination, and the value of 81 to model delamination filled with water. Then, one A-scan is generated for each simulated model using a 2.0 GHz antenna frequency. For convenience in comparison, the A-scans obtained from the two models are stacked together and plotted in Fig. 10. As can be seen, in agreement with the above assumption, the waveform reflected from the water-filled delamination is much stronger than the one reflected from the air-filled delamination.

3.5. The effect of dielectric constant of concrete

It should be noted that the dielectric constant of concrete may also affect the strength of signals reflected from delamination. To be specific, in the case of air-filled delamination, the lower the dielectric constant of concrete, the smaller will be the dielectric contrast between concrete and air, and accordingly, the reflection coefficient. On the other hand, for water-filled delamination, the higher the dielectric constant of concrete, the smaller will be the dielectric contrast between concrete and water. However, such a variation in dielectric contrast will not significantly impact the detectability of concrete delamination. Fig. 11 illustrates that when the simulation setup in Fig. 4 is used again in which two extreme values of dielectric constant of concrete (5 and 11) are used in turn for the simulation. As can be seen, while the delamination on the left (when dielectric constant of concrete is equal to 5) does not appear as strong as the one on the right (when dielectric constant of concrete is equal to 11), one can still observe the reflected signals.

3.6. The effect of delamination width

It is reasonable to assume that delamination's width or size will affect its detectability in the GPR image. Therefore, a simulation experiment (shown in Fig. 12a) has been set up to verify such an assumption. As can be seen, three air-filled delaminations of varying width were embedded in the simulation model with the value being equal to 2 cm, 4 cm, and 8 cm, respectively. All three simulated delaminations had the same thickness of 1 mm. Similar to the previous simulations, the dielectric constant of concrete was assigned a typical value of 8 and Ricker wavelet with a peak frequency of 2 GHz was utilized for transmitted signals. The B-scan image obtained is presented in Fig. 12b. As one can observe, although the reflections from three delaminations vary in shape and a bit in the strength of reflected signals, they all appear quite clearly. The delamination of the smallest size has a signature similar to those of point-like objects such as rebars, pipes or cables. That may cause some difficulty in differentiating delamination from such objects. However, based on this experiment, one can

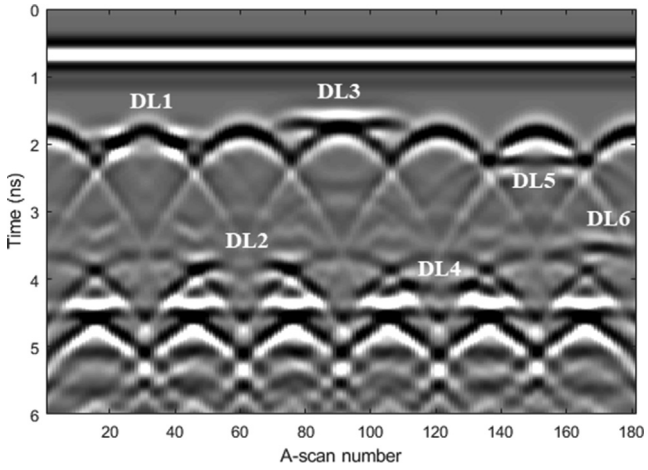

Fig. 14. Simulated B-scan obtained for 3-mm thick delaminations.

Fig. 15. Photo of the concrete slab specimen.

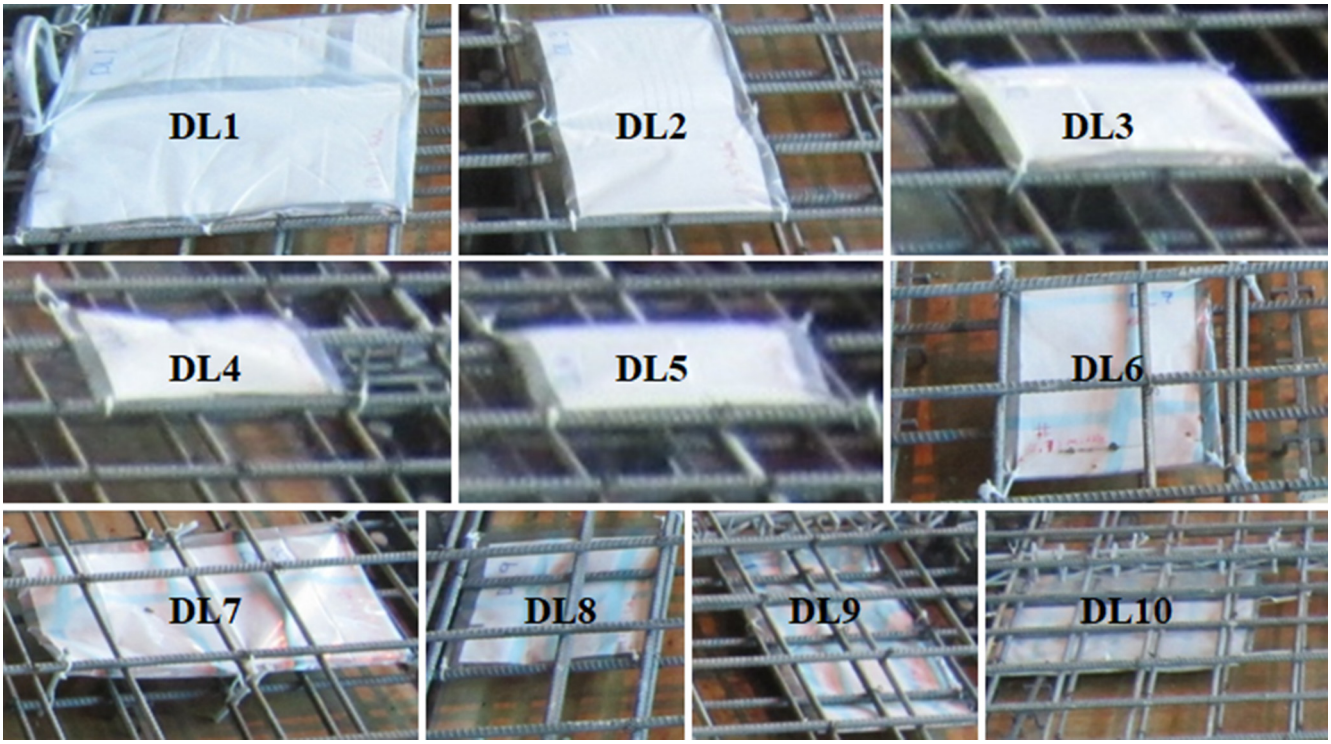

Fig. 16. Photos of simulated delaminations.

Table 1
List of simulated delaminations.

#	Width (cm)	Length (cm)	Depth (cm)
DL1	61	61	5
DL2	30.5	61	5
DL3	30.5	30.5	5
DL4	30.5	30.5	5
DL5	30.5	30.5	5
DL6	30.5	30.5	10
DL7	30.5	61	10
DL8	30.5	30.5	17
DL9	30.5	61	17
DL10	61	61	17

say that, for typical delamination, the width will not have a big impact on its detectability.

3.7. The effect of steel bars

The presence of reinforcing bars in concrete slabs may affect the capability of GPR in detecting delamination. The reasons include the following. First, since a steel bar is a perfect reflector of electromagnetic energy, it may obstruct the traveling of GPR energy to the crack location. Second, in the case of corrosion-induced delamination, its inherent proximity with rebar may lead to a resolution problem. To better understand those effects, Fig. 13 presents two simulation setups (Fig. 13a and b) for a survey with an antenna of a 2.0 GHz peak frequency and corresponding results (Fig. 13c and 13d). For clear referencing in the following discussion, each delamination in the figure was labeled (from DL1 to DL9). Each delamination was air-filled and 1 mm thick. The steel bars were modeled as of a 12 mm diameter. As can be noticed, delamination DL1, DL3, DL5, DL7, and DL9 were to simulate delaminations created by the corrosion of top rebars. On the other hand, delaminations DL2, DL4, DL6, and DL8 were to model delaminations near the bottom rebars.

As expected, Fig. 13 shows difficulties in detecting some delaminations when steel bars are included in the simulation models. More specifically, delamination DL1 does not appear in the B-scan image, and it only leads to some distortion of the hyperbolic shape of rebar reflection. Delaminations DL5, DL8, and DL9 can only be seen partially at the locations where they are not masked by a steel bar. Delaminations DL2, DL4, and DL6 near the bottom rebars can hardly be seen. On the other hand, due to some separation from rebars, delaminations DL3 and DL7 appear very clearly. Since it has been shown previously that the detectability also depends on the thickness of delamination, additional simulations were performed by increasing the thickness of delaminations in models in Fig. 13a from 1 mm to 3 mm. The results are presented in Fig. 14. As can be observed, the effects created by delaminations DL2, DL4, and DL6 have become more visible in the B-scan.

4. Validation of simulation results on an actual concrete slab

4.1. Description of the concrete slab specimen and data collection

The results from the above numerical simulations have shown that, although there are some obstacles, GPR can undoubtedly be used as a tool for direct imaging of concrete delamination. To validate the conclusions from the numerical study, a GPR survey was conducted on a concrete slab with prefabricated/simulated delamination (Fig. 15). Specifically, the concrete specimen employed in this research was constructed at the Livingston Campus of Rutgers University to evaluate performance or validate newly developed NDE techniques or new methods of data interpretation. The concrete slab is supported by three steel beams placed on two concrete abutments. The slab is 9 m long, 3.6 m wide, and 203 mm thick. It has two layers of uncoated steel reinforcement at 50 mm and 165 mm depths, respectively. Each of the reinforcement layers consists of 13 mm diameter rebars spaced at 165 mm in the

longitudinal direction and 16 mm diameter rebars spaced at 177 mm in the transverse direction.

Concerning the current study, the concrete specimen was constructed with ten simulated delaminations (denoted as DL1 to DL10 in Fig. 16). As can be seen in Table 1, they varied in the areal extent and were embedded at different depths. Shallow delaminations were placed at a 5 cm depth, while intermediate and deep delaminations were embedded at 10 cm and 17 cm depths, respectively. The delaminations were formed using two layers of plastic foam covered by a thin plastic film. The total thickness of each artificial delamination varied between 1 mm and 1.5 mm. GPR data were collected in two perpendicular directions of the slab using both 1.6 GHz and 2.6 GHz antennas. The results are presented and discussed in the following section.

4.2. Results and discussion

a. Shallow delaminations

Fig. 17 presents B-scan images that cross the areas of the shallow delaminations (DL1-DL5). Since it is known from numerical simulations that a greater separation from steel bars will make delamination become more visible, B-scan images from both longitudinal and transverse scans were employed to detect delamination. For clarification, it is noted that steel bars in two directions of each reinforcing layer are not at the same depth. In particular, the top reinforcement is in the transverse direction. Therefore, surveying in two directions may help minimize the effects of steel bars on imaging delamination. Fig. 17 clearly illustrates this con-

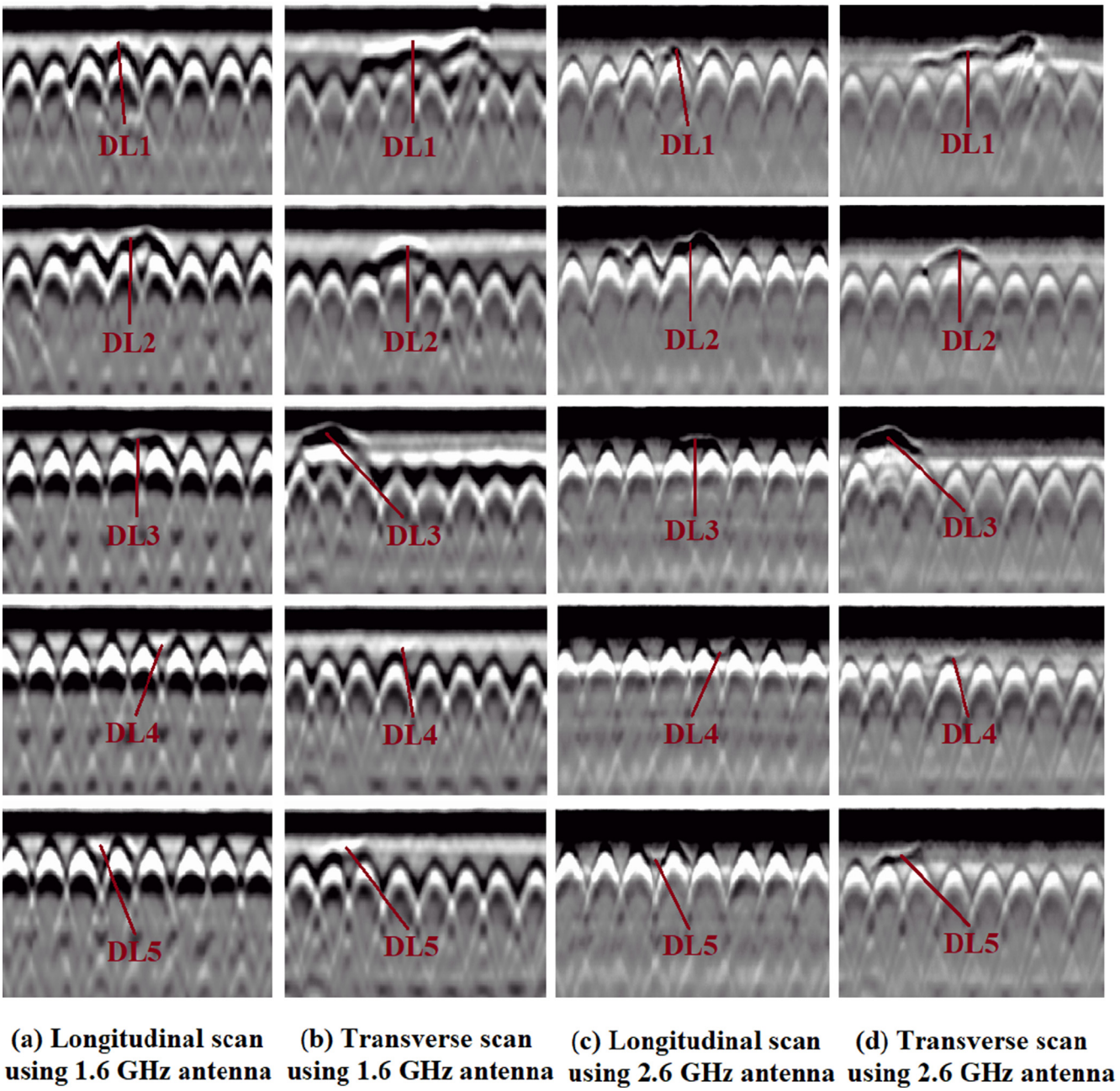

Fig. 17. Detection of shallow delaminations.

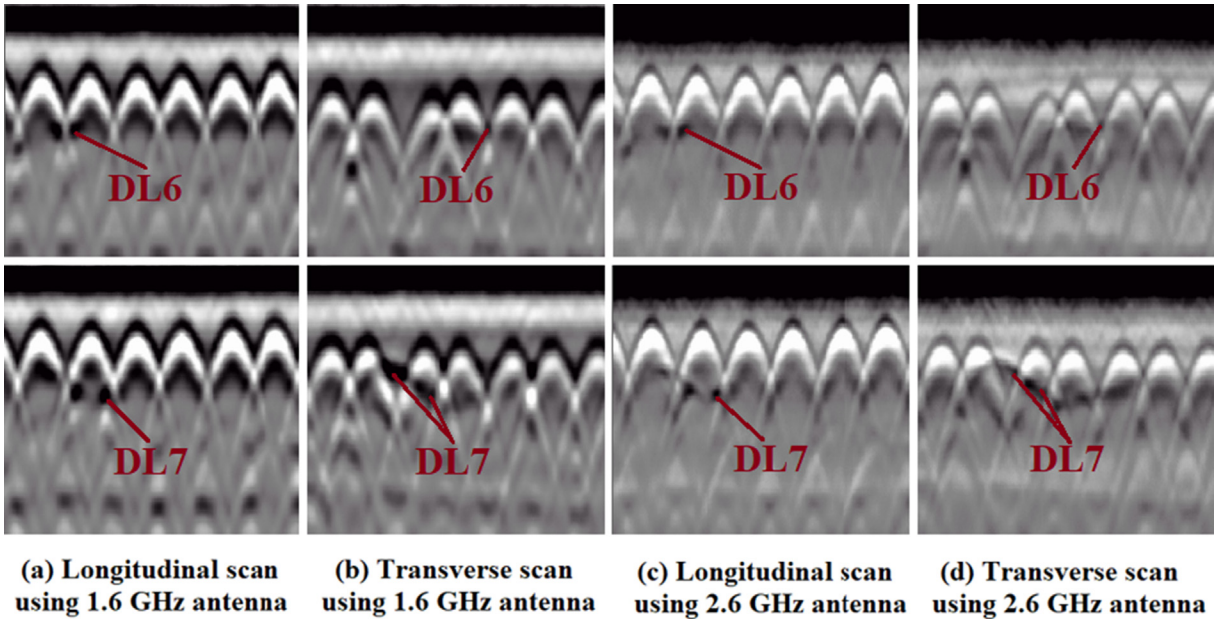

Fig. 18. Detection of intermediate delaminations.

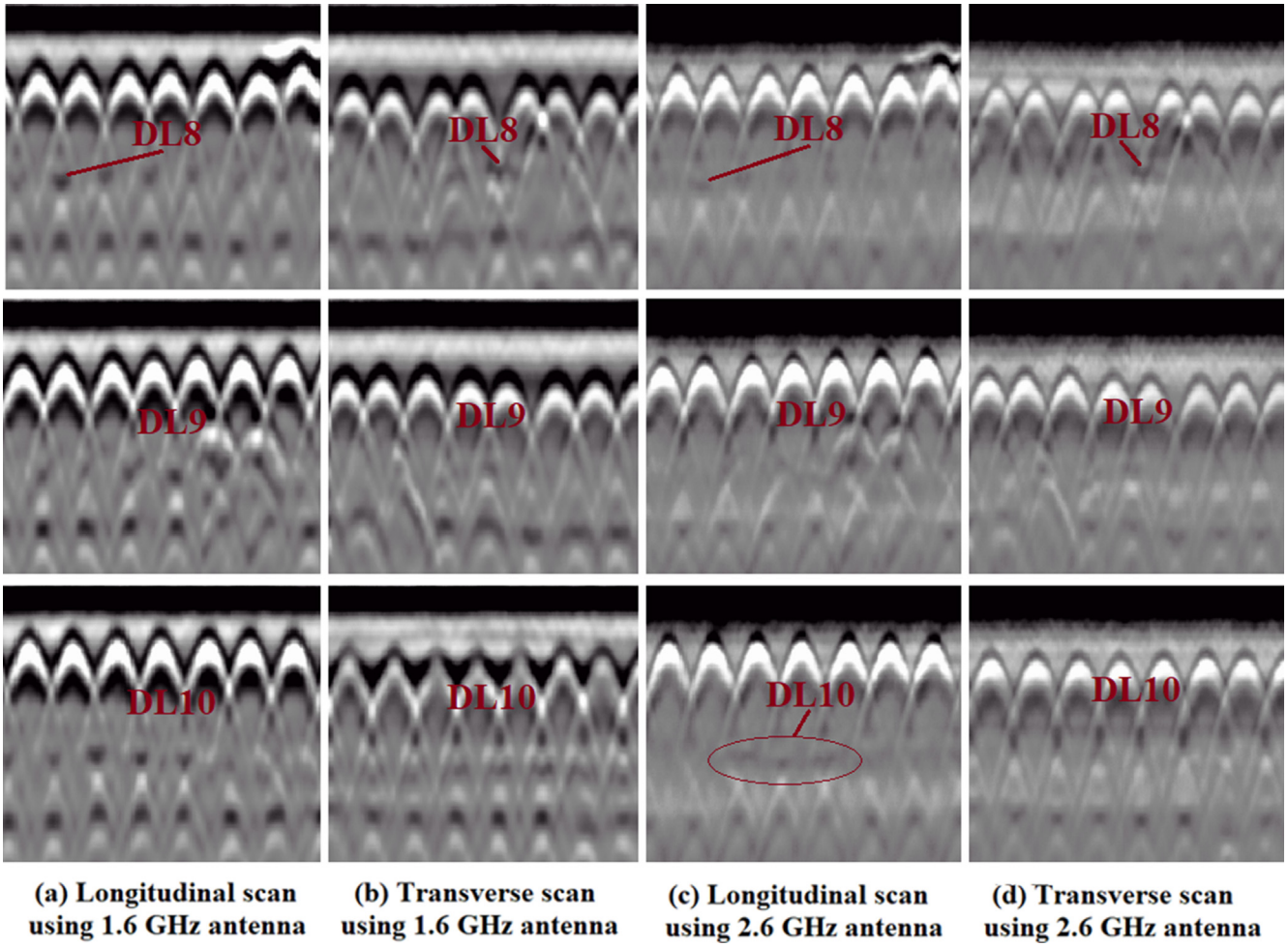

Fig. 19. Detection of deep delaminations.

cept when it is easier to detect the delaminations by using transverse B-scans rather than using longitudinal B-scans. The reason being, in the tested specimen, the shallow delaminations were placed right on top of transverse steel bars, as shown in Fig. 16. However, regardless of the scanning direction, it can be confirmed from Fig. 17 that all the shallow delaminations in the tested specimen can be imaged directly with GPR using either 1.6 GHz or 2.6 GHz antenna. The images are a bit more indicative of the presence of delamination for the 2.6 GHz antenna.

b. Intermediate delaminations

Similarly, Fig. 18 presents B-scan images from the areas with intermediate delamination (DL6 and DL7). As can be noticed, delamination DL6 is not well visible on the images from the transverse scans. However, on the longitudinal B-scans from both 1.6 GHz and 2.6 GHz antennas, it appears and has a signature similar to the results obtained from numerical simulations for delamination DL9 (Fig. 13d). Specifically, it only appears in the space between two rebars, i.e., at the tails of the hyperbolas. Concerning delamination DL7, it can be seen very clearly in all B-scan images.

c. Deep delaminations

The results from previous simulations have shown that it might be difficult to detect deep delaminations near the bottom of the slab. Fig. 19 indicates no exception for real GPR data when one can barely see on B-scan images the signs of delaminations DL8, DL9, and DL10. While this phenomenon may seem obvious, its detailed explanation is as follows. First, the area near the bottom of the slab in GPR images is very complicated to analyze with the reflections from top rebars, bottom rebars, and slab bottom. Those reflections tend to be mixed, creating complex GPR signals. Second, GPR energy reflected from deep delamination is inherently weak due to geometric, dielectric, and conductive losses [11]. As a consequence, it may be undetectable because of a reduced signal-to-noise ratio. Additionally, it is worth noting that the embedded delaminations in the tested specimen are closer to air-filled delamination. That is to say, the deep delaminations (DL8, DL9, and DL10) might have been detected if they were filled with water.

5. Conclusions

Although GPR is one of the most commonly used technologies for evaluating the condition of concrete structures, it has never been accepted as a tool to directly image concrete delamination. This study was conducted to improve understanding of the potential of GPR to detect concrete delamination and to identify the factors that may hinder the success of such an application. Based on the analysis of results obtained from numerical simulations and the data collected on an actual concrete slab, the following was concluded. First, as long as electromagnetic energy is strong enough to reach delamination, some of the energy will be reflected. The strength of such energy will depend on the thickness of delamination, whether it is air- or water-filled, on the peak frequency of the emitted signal, and to some extent, on the dielectric constant of concrete and the width of delamination. More specifically, based on numerical simulations, delamination in unreinforced concrete will likely be detected if the ratio between the wavelength of signal in concrete and delamination thickness is less than 50. Second, the depth of delamination and its position relative to neighboring steel bars impact its visibility in GPR images.

CRediT authorship contribution statement

Kien Dinh: Conceptualization, Methodology, Data curation, Writing - original draft. **Nenad Gucunski:** Writing - review & editing.

Declaration of Competing Interest

The authors declare that they have no known competing financial interests or personal relationships that could have appeared to influence the work reported in this paper.

References

[1] ASTM D6087–08(2015) e1, Standard Test Method for Evaluating Asphalt-Covered Concrete Bridge Decks Using Ground Penetrating Radar, ASTM International (2015), https://doi.org/10.1520/D6087-08R15E01.
[2] Nenad Gucunski, Arezoo Imani, Francisco Romero, Soheil Nazarian, Deren Yuan, Herbert Wiggenhauser, Parisa Shokouhi, Alexander Taffe, Doria Kutrubes (Eds.), Nondestructive Testing to Identify Concrete Bridge Deck Deterioration, Transportation Research Board, Washington, D.C., 2012.
[3] Dan G. Zollinger, Sanjaya P. Senadheera, Tianxi Tang, Spalling of Continuously Reinforced Concrete Pavements, J. Transp. Eng. 120 (3) (1994) 394–411, https://doi.org/10.1061/(ASCE)0733-947X(1994)120:3(394).
[4] Scott M, Rezaizadeh A, Moore M. Phenomenology study of HERMES ground-penetrating radar technology for detection and identification of common bridge deck features. No. FHWA-RD-01-090. 2001.
[5] S. Yehia, O. Abudayyeh, S. Nabulsi, I. Abdelqader, A Comparison Between Ground Penetrating Radar (GPR) and Impact Echo (IE) for Detection of Common Concrete Bridge Decks Defects. Computing, Civil Eng. (2005) 1–7, https://doi.org/10.1061/40794(179)34.
[6] Ali A. Sultan, Glenn A. Washer, Reliability Analysis of Ground-Penetrating Radar for the Detection of Subsurface Delamination, J. Bridge Eng. 23 (2) (2018) 04017131, https://doi.org/10.1061/(ASCE)BE.1943-5592.0001182.
[7] Juanyu Liu, Dan G. Zollinger, Robert L. Lytton, Detection of Delamination in Concrete Pavements Using Ground-Coupled Ground-Penetrating Radar Technique, Transport. Res. Record 2087 (1) (2008) 68–77, https://doi.org/10.3141/2087-08.
[8] Kien Dinh, Nenad Gucunski, Trung H. Duong, An algorithm for automatic localization and detection of rebars from GPR data of concrete bridge decks, Automat. Construct. 89 (2018) 292–298, https://doi.org/10.1016/j.autcon.2018.02.017.
[9] K. Dinh, N. Gucunski, T.H. Duong, Migration-based automated rebar picking for condition assessment of concrete bridge decks with ground penetrating radar, NDT and E Int. 1 (98) (2018) 45–54, https://doi.org/10.1016/j.ndteint.2018.04.009.
[10] Alexander Tarussov, Marc Vandry, Aldo De La Haza, Condition assessment of concrete structures using a new analysis method: Ground-penetrating radar computer-assisted visual interpretation, Constr. Build. Mater. 38 (2013) 1246–1254, https://doi.org/10.1016/j.conbuildmat.2012.05.026.
[11] K. Dinh, N. Gucunski, J. Kim, T.H. Duong, Understanding depth-amplitude effects in assessment of GPR data from concrete bridge decks, NDT and E Int. 31 (83) (2016) 48–58, https://doi.org/10.1016/j.ndteint.2016.06.004.
[12] R.P. Feynman, R.B. Leighton, M. Sands, The Feynman Lectures on Physics, Vol. 2: Mainly Electromagnetism and Matter. Addison-Wesley, 1979.
[13] K. Yee, Numerical solution of initial boundary value problems involving Maxwell's equations in isotropic media, IEEE Trans. Antennas Propag. 14 (3) (1966) 302–307, https://doi.org/10.1109/TAP.1966.1138693.
[14] A. Taflove, S.C. Hagness, Computational electrodynamics: the finite-difference time-domain method, Artech house, 2005.
[15] D.M. Sullivan, Electromagnetic simulation using the FDTD method, John Wiley & Sons, 2013. Doi: 10.1002/9781118646700.
[16] Jean-Pierre Berenger, A perfectly matched layer for the absorption of electromagnetic waves, J. Comput. Phys. 114 (2) (1994) 185–200, https://doi.org/10.1006/jcph.1994.1159.
[17] Yanghua Wang, Frequencies of the Ricker wavelet, Geophysics 80 (2) (2015) A31–A37, https://doi.org/10.1190/geo2014-0441.1.
[18] Kien Dinh, Tarek Zayed, Francisco Romero, Alexander Tarussov, Method for Analyzing Time-Series GPR Data of Concrete Bridge Decks, J. Bridge Eng. 20 (6) (2015) 04014086, https://doi.org/10.1061/(ASCE)BE.1943-5592.0000679.